Elastic scattering and vibrational excitation of CO_2 by 4, 10, 20 and 50 eV electrons

1980 J. Phys. B: At. Mol. Phys. 13 1651

(http://iopscience.iop.org/0022-3700/13/8/019)

J. Phys. B: Atom. Molec. Phys. **13** (1980) 1651–1662. Printed in Great Britain

Elastic scattering and vibrational excitation of CO_2 by 4, 10, 20 and 50 eV electrons†

D F Register, H Nishimura‡ and S Trajmar

Jet Propulsion Laboratory, California Institute of Technology, Pasadena, California 91103, USA

Received 25 September 1979

Abstract. Elastic and vibrationally inelastic differential, integral and momentum-transfer cross sections for electrons scattered by CO_2 molecules are reported at 4, 10, 20 and 50 eV impact energies. The elastic cross sections are placed on an absolute scale by means of a relative flow technique. The inelastic cross sections are normalised to the elastic ones by using the inelastic to elastic intensity ratios. Data are reported for up to ten features in the 0·0 to 0·4 eV energy-loss region.

1. Introduction

Data concerning low to intermediate energy scattering of electrons by CO_2 is of significant practical interest for modelling high-power infrared CO_2 lasers as well as for understanding upper atmospheric processes. Despite this interest, very little experimental or theoretical data are available for differential cross sections (DCS) in the few eV to 50 eV impact energy range. Danner (1970) has studied low energy e^-–CO_2 elastic and vibrationally inelastic processes, but this experimental data remains unpublished. Shyn *et al* (1978) has reported experimental DCS for elastic scattering from 2 to 90 eV. R T Poe, B H Choi and J Sun (1979, private communication) have performed two-potential calculations for e^-–CO_2 elastic and vibrationally inelastic scattering for impact energies of 50 eV and above. Morrison *et al* (1977) have published calculations for low-energy differential cross sections and Onda and Truhlar (1979) have recently reported DCS and integral cross section calculations for e^-–CO_2 elastic scattering at 20 eV.

We report here the results of a survey of e^-–CO_2 elastic and vibrationally inelastic scattering at impact energies of 4, 10, 20 and 50 eV. The energy-loss region studied was 0 to 0·4 eV which included at least 11 observed transitions. The low impact energy range of the present work was chosen to overlap with Danner's data (1970) while the high-energy limit was chosen to overlap the calculations of Poe *et al* (1979, private communication). At all energies, comparison can be made with the elastic DCS of Shyn *et al* (1978). The elastic DCS were placed on an absolute scale by means of a relative flow technique (Srivastava *et al* 1975) and the recently measured He elastic DCS of Register *et al* (1979). The inelastic cross sections were normalised to the elastic cross sections by using the measured inelastic to elastic intensity ratios.

† Work supported by NASA Contract No NAS7-100.

‡ NRC-NASA Senior Resident Research Associate. Permanent address: Department of Physics, Niigata University, Niigata 950-21, Japan.

0022-3700/80/081651+12$01.50

2. Experimental procedure

The electron impact spectrometer has been described previously (Jensen 1978). It consists of a magnetically shielded vacuum chamber containing a double hemispherical electron source and detector systems. All lenses in the electron optics are of a cylindrical design and are constructed of gold-plated oxygen-free copper with 0·005 in thick molybdenum aperture plates. The electron gun is differentially pumped to reduce space charge, filament cooling and other gas-dependent effects in the incident electron beam. The energy-selected scattered electrons are detected by a Bendix 4219 channeltron. The channeltron pulses are amplified and recorded in an ND600 multichannel analyser. The data obtained is transferred to a Tektronix 4051 microprocessor system for final analysis and storage.

The gas flow system is shown in figure 1. Two Matheson mass flow meters (F-1 A, B—one for each gas) are used to avoid gas contamination problems in the flow meters. The flow meters are placed in the high-pressure section of the gas line to improve their response time, stability and calibration accuracy. The gas line length from valves V-2 (A and B) to the Wallace Tiernan (WT) pressure gauge (M-2) was cut to identical lengths in order to cross calibrate accurately the flow meters. Valves V-7 and V-8 direct the flow to either the capillary array (target) or a side leak which was used for correcting direct beam and background contributions to the scattered signal.

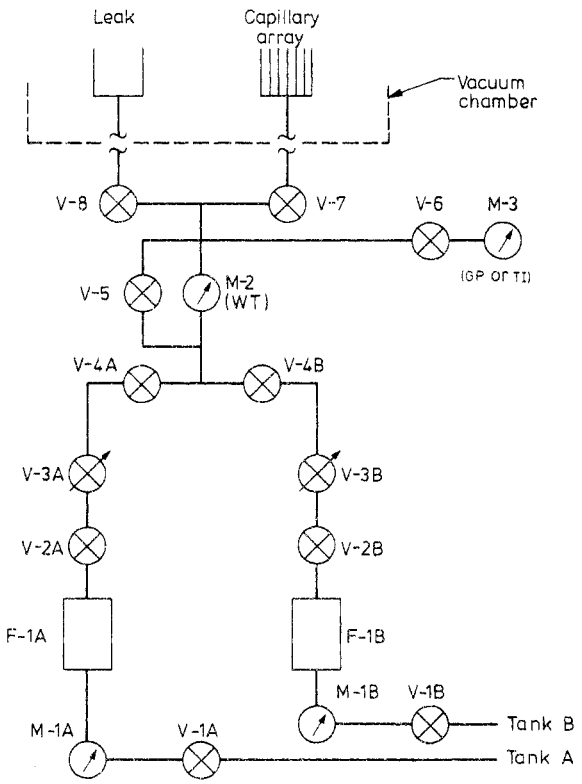

Figure 1. CO_2/He gas flow system: V indicates valves (⊗ = shut-off; ⊕ = needle or throttling valve), M indicates pressure meters, F-1 A and B are the flow meters.

The recent calculations of Brinkman and Trajmar (1979) have demonstrated that for molecular and quasi-molecular flow in capillary arrays the relative density distribution of capillary array sources is not especially sensitive to the gas Knudsen number. Therefore, as long as the Knudsen numbers for the two gases are approximately equal the density distributions for the two gases will be essentially identical. The basic problem in the relative flow method then becomes one of calibrating the flow meters and pressure gauges.

The calibration of the Wallace Tiernan gauge was made by replacing the high-pressure Granville Phillips gauge (M-3) by a Texas Instruments (TI) crystal quartz manometer. The vacuum system and gas lines were then pumped to a pressure of 2×10^{-8} Torr to outgas the system properly and to define the true zero of the meters. CO_2 pressure readings were then made on the two meters up to 15 Torr. Gas diffusion in the TI gauge did not permit a similar calibration for He. However, since the WT gauge uses a simple diaphragm pressure measuring system, a calibration on CO_2 will yield a proper reading for any other gas (including He).

For cross calibrating the flow meters, the TI gauge was removed from the system and the Wallace Tiernan used as the standard. Each flow meter was checked for linearity by establishing first the desired flow rate in the system through the side leak. The pressure and flow rate were recorded and the leak valve was then closed. The time required for the Wallace Tiernan gauge to reach 15 Torr was then measured and the process repeated for a different flow rate. Since the flow under these conditions is into a fixed volume, the pressure reading is simply a static pressure and should be directly proportional to the product of the flow rate and the time. Using this procedure it was found that the two flow meters were linear to within $\pm 2\%$ over an operating range of 0·1 to 2 standard cubic centimetres per minute (SCCM).

Finally, assuming the ideal gas law to be correct the ratio of the product of flow times time for the two gases should yield the ratio of gas correction factors for the two flowmeters. Again using 15 Torr for the final pressure, this ratio was determined and was found to agree with the manufacturer's calibration to within $\pm 2\%$. The advantage of this type of calibration lies in the fact that it is performed with the system under actual operating conditions and does not require any external reference or modification of the gas flow apparatus. For these reasons, it is felt that this calibration procedure determines the relative gas target densities to any accuracy of better than 5%.

Typical back pressures and flow rates for the two gases were 4 Torr and 0·6 SCCM for He and 1 Torr and 0·2 SCCM for CO_2. Under these conditions quasi-molecular flow in the capillary array was obtained and the Knudsen number for the two gases was nearly identical. The background correction to the elastic scattering was typically less than 5% for large angle scattering ($\theta > 40°$) and up to 30% at the lowest measured angles and energies (20°, 4 eV). The system energy resolution for these measurements was 20–23 meV which provided good separation of the 0·083 eV energy-loss feature from the elastic peak. Typical energy-loss spectra at 4 and 20 eV are shown in figures 2 and 3.

In spite of the excellent resolution in the present measurements, some inelastic features are not resolvable. In particular, the Σ_g^+ transitions at 0·159 eV (02^00) and 0·172 eV (10^00) are not resolved in these experiments. In order to define these and other cross sections more precisely, an unfolding program was developed. The procedure used was to determine the energy levels for CO_2 using the known spectroscopic constants for this molecule. The shape of the elastic feature was then applied to the calculated positions of each of the transitions of interest. A possible objection to this method is that rotational transitions and direct beam may broaden the elastic feature

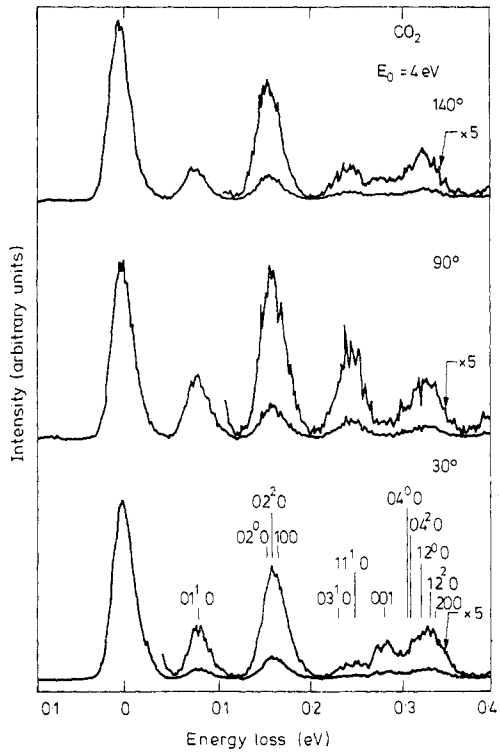

Figure 2. $e^- - CO_2$ energy-loss spectra at 4 eV impact energy and scattering angles of 30°, 90° and 140°.

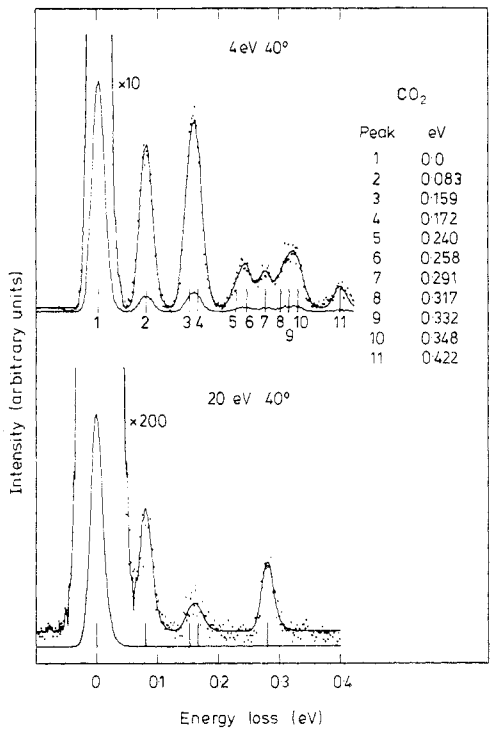

Figure 3. Data and fit for 40° energy-loss spectra at 4 and 20 eV. The full curve is the fit to the data points.

more than the inelastic. However, in all spectra two inelastic features are usually completely resolved, 0·083 eV (01^10) and 0·291 eV (00^01), and the elastic shape was found to give a near perfect fit to both of these peaks. A complete list of the unfolded energies as well as typical fits are given in figure 3. At the higher energies only features 1, 2, 3, 4 and 7 were included in the program. In all cases, Δ states were not considered in the fitting. At the higher energies $\Delta l = 2$ transition cross sections are typically very small while at 4 eV, the calculations of Morrison *et al* (1977) indicate that Δ state integral cross sections are several orders of magnitude smaller than those for Σ and Π states.

3. Results and discussion

The errors in the present measurements are a combination of the statistical, systematic and normalisation errors in the experiments (e.g. $\bar{X} = (X_1^2 + X_2^2 + \ldots)^{1/2}$). In addition to the estimated 5% error in the flow system, drift in the electron gun and background scattering also contribute to the normalisation uncertainties. The background correction is made at each energy and angle by directing the gas flow to either the capillary array or the sideleak. As the total background correction is typically 5% (with a worst case of 30% at 4 eV, 20°), the error from this source is probably negligible. Electron gun drift was monitored by observing the Faraday cup current and scattering intensity at

a given scattering angle before and after the elastic DCS measurements. In all cases, drift was found to be less than 5%. Combining these instrumental errors with the estimated 5% uncertainty in the He DCS gives a total normalisation error of about 10%.

In addition to the normalisation errors, the elastic DCS may be affected by systematic errors in measuring the angular distribution. At the lower energies, a significant contribution to the detected elastic intensity can arise from the strong 0·083 eV energy-loss feature. At higher energies, uncertainty in the angular position by as little as 1° can introduce an error in the DCS of up to 10%. In the present measurements, the mechanical angular position is reproducible to 0·1° but electron beam drift and focusing may introduce an angular uncertainty of up to 0·5°. Although the symmetry of the elastic DCS about 0° and the 0·083 eV energy-loss contribution have been checked, a residual uncertainty in the DCS of less than 10% may still arise from these contributions. Therefore, the elastic DCS at each energy is accurate to approximately 15% due to the combination of all the considered errors.

For the inelastic cross sections the errors in the measurement of the inelastic intensities must be folded with the estimated 15% error in the normalisation of the elastic DCS. The inelastic DCS are typically 2–4 orders of magnitude smaller than the elastic ones at the higher energies. Thus the inelastic statistical errors are the largest contribution to the uncertainties in these cross sections.

From 2–4 measurements of the energy-loss spectra were made at each angle for impact energies of 4, 10 and 20 eV. At 50 eV two measurements were typically made but in some cases only one value of the inelastic intensity could be accepted. This is especially true of the 0·083 eV feature which, in most cases was difficult to resolve from the elastic even when the resolution was better than 20 meV. Consequently, the inelastic errors at 50 eV are appreciably larger than at the other energies. These errors are given in the tables.

The elastic DCS at 4, 10, 20 and 50 eV are presented in table 1. Comparison with the available experimental and theoretical data is given in figures 4, 10 and 11. In general, the present results are in excellent agreement with Danner's (1970) data. At 4 eV (4·2 eV for Danner), there is some disagreement with his results below 30° (see figure 4), while at 10 eV the two experiments are in excellent agreement for all the measured angles. Danner presents relative elastic angular distributions at 19·6 eV which have been normalised to the present 20 eV data at 90°. These results are again in excellent agreement with ours.

Shyn *et al*'s elastic DCS (1978) do not compare as favourably with our data. At 10 eV the agreement is quite good, but at the other energies (figures 4, 10 and 11) their results are systematically higher and more forward peaked. Since Shyn *et al* calibrate their data at 10 eV and then apply a correction derived from this calibration to the other energies, the discrepancy may arise because of systematic errors in this technique. At 4 eV another consideration is the presence of the strong 0·083 eV transition which may not be well resolved in their work. As this feature has a cross section as large as 40% of the elastic, this correction is by no means insignificant.

Comparison is made in figure 10 with Onda and Truhlar's (1979) calculation at 20 eV and in figure 11, Poe *et al*'s two-potential calculations (1979) at 50 eV. In both cases theory produces cross sections which are larger than the experimental results but which agree quite reasonably with the shape of the angular distributions.

The vibrationally inelastic DCS are given in tables 2–5 and are compared with Danner's (1970) and Poe *et al*'s (1979) results in figures 5–9 and 12 respectively. The strongest inelastic features (0·083 eV—01^10 and 0·291 eV—00^01) at 4 eV are in

Table 1. CO_2 elastic DCS ($Å^2\,sr^{-1}$). DCS and integral cross section uncertainties are 15% and 20% respectively. ( ) indicates an extrapolated value.

θ	4 eV	10 eV	20 eV	50 eV
0	(2·8)	(4·5)	(10·2)	(22·6)
5	(2·5)	(3·65)	(9·4)	(14·8)
10	(2·2)	(3·08)	(7·2)	(9·7)
15	(1·92)	2·68	5·43	6·35
20	1·68	2·21	4·59	4·45
30	1·3	1·5	2·61	1·71
40	1·03	1·21	1·58	0·74
50	0·86	0·96	0·94	0·34
60	0·75	0·73	0·62	0·19
70	0·64	0·59	0·42	0·15
80	0·52	0·52	0·3	0·113
90	0·44	0·45	0·27	0·1
100	0·38	0·43	0·32	0·094
110	0·36	0·45	0·43	0·138
120	0·37	0·53	0·55	0·267
130	0·44	0·73	0·68	0·4
140	0·64	0·96	0·91	0·7
150	(0·84)	(1·21)	(1·2)	(0·98)
160	(1·04)	(1·47)	(1·5)	(1·3)
170	(1·24)	(1·74)	(1·75)	(1·55)
180	(1·44)	(1·98)	(1·95)	(1·7)
Q_I	8·73	10·61	12·32	8·75
Q_M	7·34	9·52	8·89	5·55

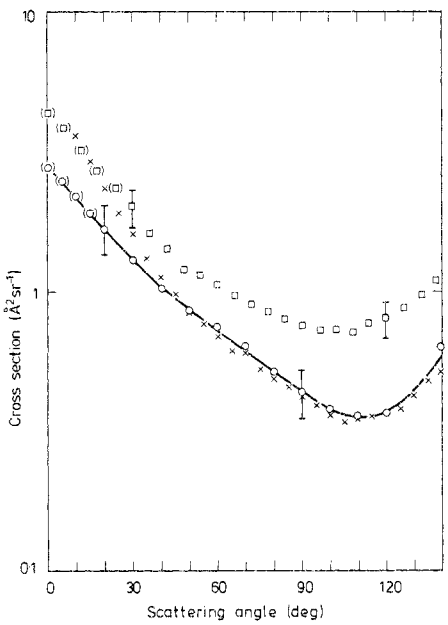

Figure 4. 4 eV elastic DCS for CO_2: -○-, present data; ×, Danner (1970) at 4·2 eV; □, Shyn *et al* (1978).

Table 2. CO_2 vibrationally inelastic DCS ($Å^2\ sr^{-1}$) for 4 eV impact energy. DCS and integral cross section uncertainties are 20% and 25% respectively.

θ	0·083	0·159	0·172	Sum	0·240	0·258
0	(78)	(0·2)	(0·23)	(0·43)	—	—
5	(1·11)	(0·19)	(0·22)	(0·41)	—	—
10	0·281	0·157	0·191	0·348	—	—
15	0·131	0·185	0·227	0·412	0·0035	0·0045
20	0·066	0·135	0·164	0·299	0·0069	0·0088
30	0·07	0·088	0·107	0·195	0·0094	0·0162
40	0·088	0·05	0·061	0·111	0·0108	0·0207
50	0·107	0·037	0·041	0·078	0·0148	0·0235
60	0·133	0·036	0·039	0·075	0·0163	0·0268
70	0·143	0·035	0·039	0·074	0·0169	0·0292
80	0·147	0·038	0·038	0·076	0·0157	0·0307
90	0·151	0·044	0·041	0·085	0·0185	0·0304
100	0·147	0·053	0·050	0·103	0·0177	0·03
110	0·15	0·068	0·051	0·119	0·0161	0·0262
120	0·132	0·069	0·043	0·112	0·0141	0·0238
130	0·112	0·063	0·038	0·101	0·0119	0·0196
140	0·110	0·057	0·040	0·097	0·0104	0·0173
150	(0·097)	(0·05)	(0·037)	(0·087)	—	—
160	(0·083)	(0·042)	(0·032)	(0·074)	—	—
170	(0·068)	(0·033)	(0·028)	(0·061)	—	—
180	(0·055)	(0·027)	(0·023)	(0·050)	—	—
Q_I	1·70	0·70	0·64	1·34		
Q_M	1·57	0·66	0·53	1·19		

θ	Sum	0·291	0·317	0·332	0·348	Sum
0	—	(19·0)	(0·033)	(0·14)	(0·1)	(0·273)
5	—	(3·0)	(0·03)	(0·12)	(0·09)	(0·24)
10	—	0·85	0·02	0·114	0·052	0·1855
15	0·008	0·389	0·026	0·073	0·074	0·173
20	0·0167	0·141	0·0143	0·0694	0·049	0·133
30	0·0256	0·047	0·0127	0·037	0·036	0·086
40	0·0315	0·016	0·0093	0·0173	0·0217	0·0483
50	0·0383	0·0066	0·0044	0·0132	0·0148	0·0324
60	0·0431	0·0045	0·0052	0·0134	0·0129	0·0315
70	0·0461	0·0029	0·0054	0·0127	0·0127	0·0308
80	0·0464	0·0025	0·0062	0·0145	0·0118	0·0325
90	0·0489	0·0024	0·0078	0·016	0·0134	0·0372
100	0·0477	0·0022	0·0101	0·0207	0·015	0·0458
110	0·0423	0·0034	0·0133	0·0225	0·0192	0·0550
120	0·0379	0·0043	0·0099	0·0235	0·0166	0·0500
130	0·0315	0·0069	0·0099	0·0154	0·0173	0·0426
140	0·0277	0·0125	0·0073	0·0167	0·0147	0·0387
150	—	(0·021)	(0·0055)	(0·0134)	(0·0122)	(0·0311)
160	—	(0·033)	(0·0036)	(0·0109)	(0·0094)	(0·0239)
170	—	(0·05)	(0·0024)	(0·0081)	(0·0069)	(0·0174)
180	—	(0·073)	(0·0016)	(0·0059)	(0·0056)	(0·0131)
Q_I		0·511	0·106	0·256	0·219	0·581
Q_M		0·129	0·103	0·211	0·188	0·502

Table 3. CO_2 vibrationally inelastic DCS ($Å^2\,sr^{-1}$) for 10 eV impact energy. DCS and integral cross section uncertainties are 20% and 25% respectively.

θ	0·083	0·159	0·172	Sum	0·291	0·325
0	(36·6)	(0·04)	(0·025)	(0·065)	(30·9)	(0·0012)
5	(0·311)	(0·033)	(0·021)	(0·54)	(0·86)	—
10	0·078	0·0269	0·0159	0·0428	0·22	0·0015
15	0·0339	0·0222	0·0142	0·0364	0·0836	—
20	0·0168	0·0208	0·0106	0·0314	0·0336	0·0018
30	0·0065	0·0158	0·0092	0·025	0·0089	0·0017
40	0·0044	0·0132	0·0073	0·0205	0·004	0·0016
50	0·0038	0·0111	0·0064	0·0175	0·0031	0·0014
60	0·0058	0·0099	0·0053	0·0152	0·0031	0·0013
70	0·0087	0·0091	0·0051	0·0142	0·0026	0·0011
80	0·0111	0·0087	0·0057	0·0144	0·0028	0·0012
90	0·0120	0·0089	0·0051	0·0140	0·0026	0·0011
100	0·0126	0·009	0·005	0·0140	0·0027	0·0012
110	0·0117	0·0086	0·0052	0·0138	0·0032	0·001
120	0·0092	0·0096	0·0052	0·0148	0·004	0·0012
130	0·0084	0·0111	0·0056	0·0167	0·0052	0·0014
140	0·0077	0·0126	0·0064	0·019	0·0064	0·0019
150	(0·0067)	(0·0133)	(0·0064)	(0·0197)	(0·0076)	(0·0021)
160	(0·0054)	(0·0137)	(0·0065)	(0·0202)	(0·0087)	(0·0024)
170	(0·0044)	(0·0137)	(0·0063)	(0·02)	(0·0096)	(0·0026)
180	(0·0034)	(0·0135)	(0·0059)	(0·0194)	(0·0103)	(0·0028)
Q_I	0·171	0·140	0·077	0·217	0·185	0·017
Q_M	0·114	0·133	0·071	0·204	0·059	0·018

Table 4. CO_2 vibrationally inelastic DCS ($Å^2\,sr^{-1}$) for 20 eV impact energy. DCS and integral cross section uncertainties are 25% and 30% respectively.

θ	0·083	0·159	0·172	Sum	0·291
0	(351·4)	—	—	(0·018)	(63·4)
5	(0·2)	—	—	(0·012)	(0·44)
10	0·05	0·0034	0·0052	0·0086	0·112
20	0·01	0·0014	0·0023	0·0037	0·0129
30	0·005	0·0009	0·0009	0·0018	0·0031
40	0·0043	0·00052	0·00058	0·0010	0·0024
50	0·0042	0·00039	0·00071	0·0011	0·0022
60	0·0043	0·00039	0·00043	0·00082	0·002
70	0·004	0·00028	0·00055	0·00083	0·0019
80	0·0036	0·0004	0·00045	0·00085	0·0017
90	0·0036	0·00046	0·00031	0·00077	0·0012
100	0·0041	0·0004	0·00042	0·00082	0·0012
110	0·0057	0·00035	0·00038	0·00073	0·0015
120	0·0077	0·00035	0·00051	0·00086	0·0023
130	0·0098	0·00035	0·00046	0·00081	0·0029
135	0·0117	0·00041	0·00024	0·00065	0·0031
140	(0·013)	—	—	(0·0007)	(0·0033)
150	(0·017)	—	—	(0·0007)	(0·0038)
160	(0·022)	—	—	(0·0007)	(0·0042)
170	(0·025)	—	—	(0·0007)	(0·0049)
180	(0·028)	—	—	(0·0007)	(0·0056)
Q_I	0·135			0·014	0·11
Q_M	0·112			0·010	0·031

Table 5. CO_2 vibrationally inelastic DCS ($Å^2\,sr^{-1}$) for 50 eV impact energy. DCS and integral cross section uncertainties are 40% and 50% respectively.

θ	0·083(eV)	0·166(eV)	0·291(eV)
0	—	(0·014)	(61·02)
5	—	(0·0077)	(0·068)
10	—	0·00413	0·0171
20	—	0·00113	0·00466
30	—	0·0005	0·00234
40	0·00534	0·00041	0·00196
50	0·00408	0·00026	0·00136
60	0·003	0·00033	0·00093
70	0·0023	0·00044	0·00067
80	0·00222	0·00037	0·00032
90	0·0032	0·00035	0·00025
100	0·0053	0·00046	0·00021
110	0·0074	0·00054	0·00043
120	0·0099	0·0008	0·00073
130	0·012	0·00124	0·00095
140	0·020	0·0025	0·0018
150	(0·032)	(0·0049)	(0·003)
160	(0·05)	(0·009)	(0·006)
170	(0·08)	(0·018)	(0·012)
180	(0·12)	(0·035)	(0·023)
Q_I	—	0·018	0·033
Q_M	—	0·028	0·021

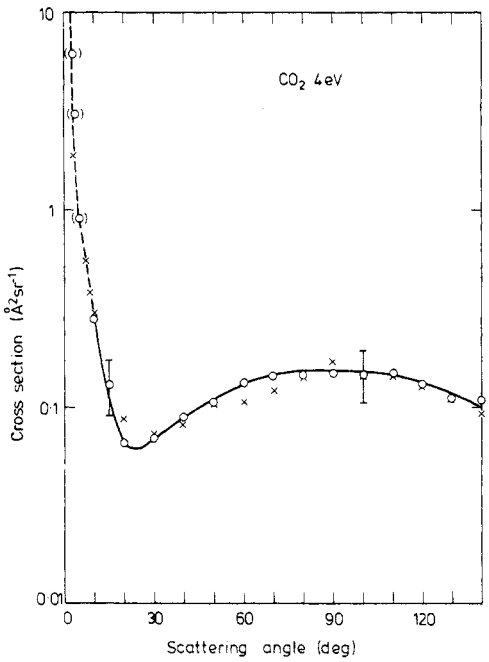

Figure 5. 0·083 eV energy-loss DCS, Π_u (01^10). $E_0 = 4$ eV: —○—, present data; ×, Danner (1970) at 4·2 eV.

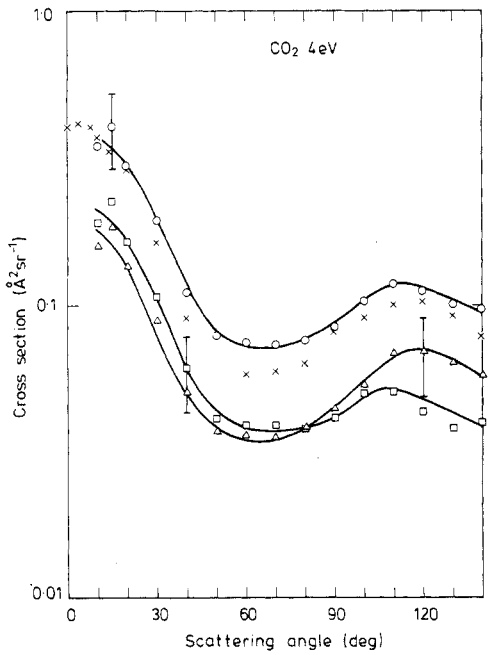

Figure 6. 0·159 and 0·172 eV DCS (and sum). $E_0 =$ 4 eV. —△—, 0·159 eV, $\Sigma_g^+(02^00)$; —□—, 0·172 eV, $\Sigma_g^+(10^00)$; —○—, sum; ×, Danner (1970) (4·2 eV, 0·167 energy loss).

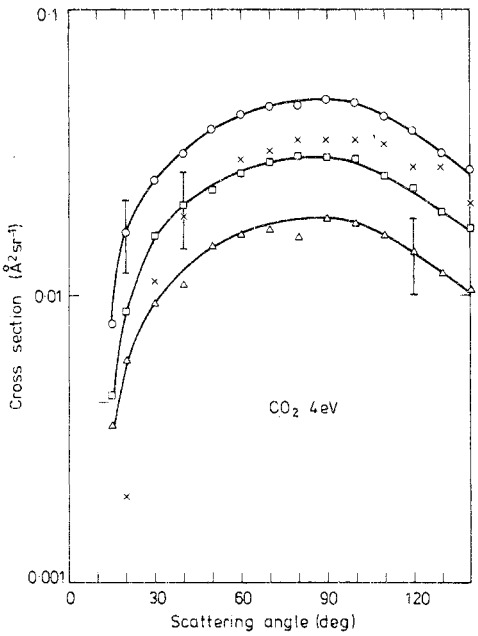

Figure 7. 0·240 and 0·258 eV DCS (and sum). $E_0 = 4$ eV. -△-, 0·240 eV $\pi_u(03^10)$; -□-, 0·258 eV $\pi_u(11^10)$; -○-, sum; ×, Danner (1970) (4·2 eV, 0·255 energy loss).

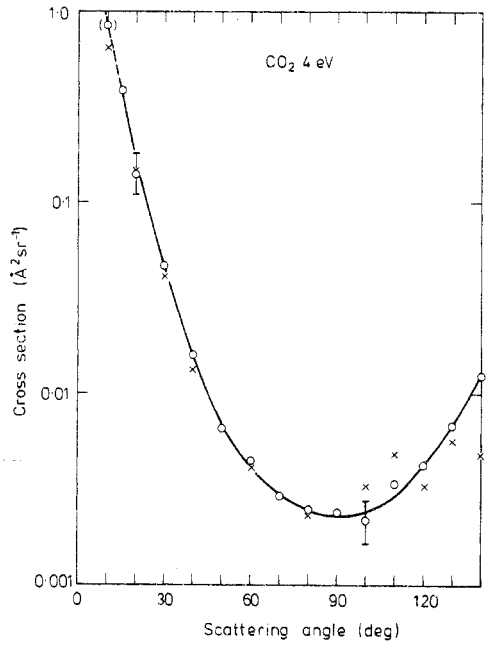

Figure 8. 0·291 eV DCS. $E_0 = 4$ eV. $\Sigma_g^+(00^01)$; -○-, present data; ×, Danner (1970) (4·2 eV).

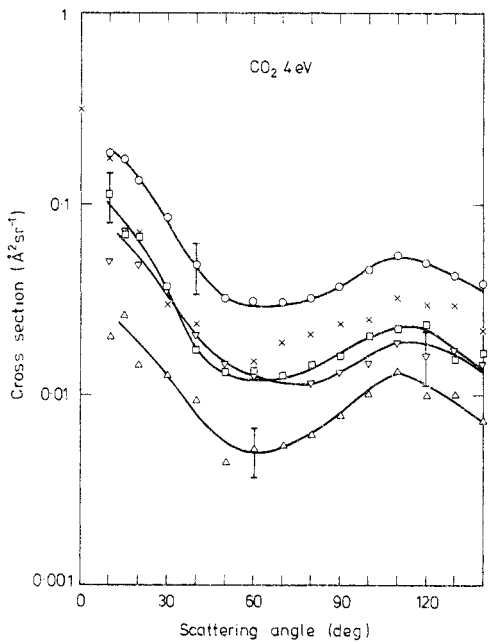

Figure 9. 0·317, 0·332 and 0·348 eV DCS (and sum). $E_0 = 4$ eV. -△-, 0·317 $\Sigma_g^+(04^00)$; -□-, 0·332 $\Sigma_g^+(12^00)$; -▽-, 0·348 Σ_g^+ (20^00); -○-, sum; ×, Danner (1970) (4·2 eV, 0·339 energy loss).

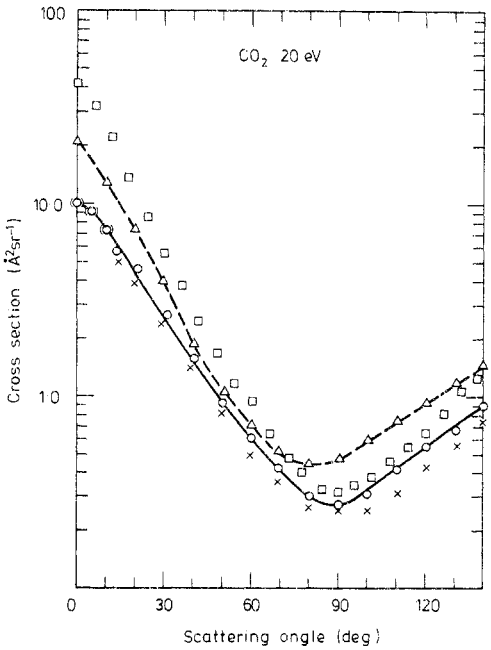

Figure 10. 20 eV elastic DCS. -○-, present data; ×, Danner (1970) (19·6 eV normalised at 90°); □, Shyn *et al* (1978); -△-, Onda and Truhler (1979) (theory).

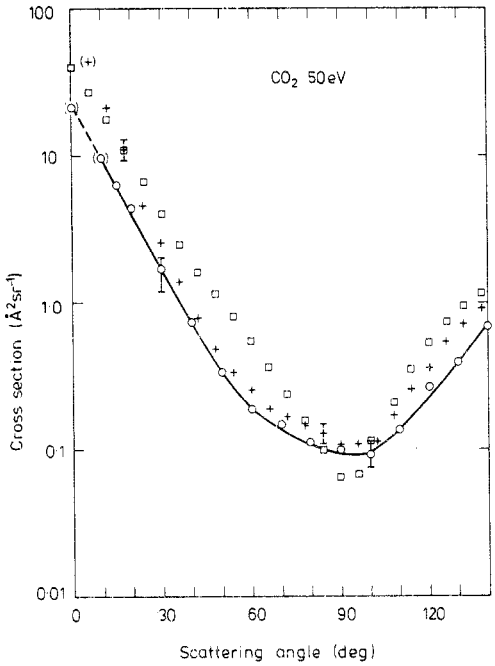

Figure 11. 50 eV elastic DCS. -○-, present data; +, Shyn *et al* (1979); □, Poe *et al* (theory).

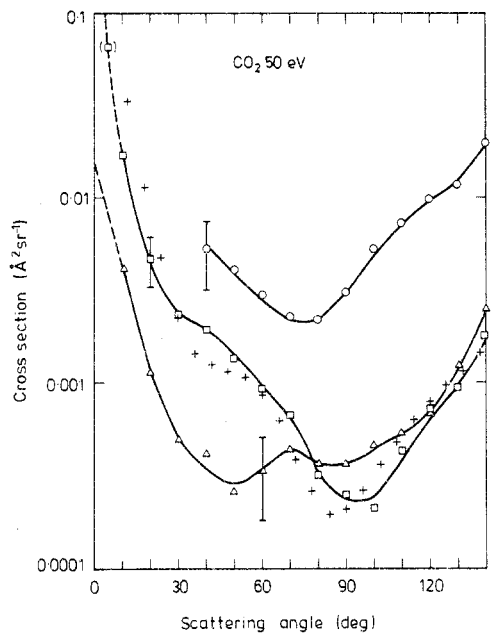

Figure 12. 0·083, 0·166 and 0·291 eV DCS. E_0 = 50 eV. -○-, 0·083 eV, $\pi_u(01^10)$; -△-, 0·166 eV (0·159+0·172), $\Sigma_g^+(02^00+10^00)$; -□-, 0·291 eV, $\Sigma_u^+(00^01)$; +, Poe *et al* (00^01) (theory).

excellent agreement with Danner's data at 4·2 eV. For the other features, the sum of unfolded transitions for the same symmetry can be compared with the corresponding composite DCS in Danner's work. For instance, the sum of the Σ_g^+ cross sections at 0·159 eV (02^00) and 0·172 eV (10^00) from the present work may be compared with Danner's 0·167 eV DCS. In all cases, the present summed DCS is systematically higher than Danner's but within the combined error bars for the two experiments. Since the completely resolved features from the two measurements are in such good agreement, this suggests that the sum of the unfolded inelastic DCS in our work may be slightly more accurate than Danner's measurements.

At 50 eV, the present vibrationally inelastic cross sections are in reasonable agreement with Poe *et al*'s (1979) two-potential calculations. Although theoretical results are available for all the experimental transitions, only the 0·291 eV (Σ_u^+—00^01) has been plotted. This feature exhibits the best agreement between theory and experiment which is, in general, within the error bars associated with our data.

Integral and momentum-transfer cross sections have been obtained for some of the excitations by extrapolating the data between 0° to 10° or 15° and 140° to 180°. These results are presented at the bottom of the corresponding tables. For some inelastic features (notably 0·083 eV and 0·291 eV), the low angle DCS is dominated by a $1/K^2$ dependence arising from an induced dipole moment (K being the momentum transfer). Other features (0·159, 0·172, 0·317, 0·332 and 0·348 eV) either do not exhibit this behaviour or it occurs at such small scattering angles that it does not contribute significantly to the integral cross section. The 0·240 and 0·258 eV features should, in principle, exhibit a strong induced dipole character. However, at 4 eV this behaviour is

not apparent down to 15° scattering angle. Either the $1/K^2$ dependence occurs at lower angles or the presence of the CO_2 resonance significantly affects the angular distribution of these states. In either case, the low-angle DCS will affect the integral cross section. Since a reasonable guide for extrapolating the DCS is not obvious, no integral or momentum-transfer cross sections are quoted for these transitions.

The estimation of the DCS from 140–180° is quite subjective. For both the elastic and inelastic transitions, this extrapolation was simply a visual continuation of the high-angle DCS curve. Where possible similarities in the shape of the present DCS with other experimental and theoretical work was used as a guide. Errors from this source may increase the uncertainty in the integral (Q_I) and momentum-transfer (Q_M) cross sections by 10% to 20%. These errors are given in the tables.

Acknowledgments

The authors would like to acknowledge fruitful discussions with Professor R T Poe, Dr B H Choi and Mr J Sun of the University of California, Riverside. We would like to thank the University of California, Riverside group for use of their e^-–CO_2 calculations prior to publication.

References

Brinkman R and Trajmar S 1979 to be published
Danner D 1970 *PhD Thesis* Physikalisches Institute der Universitat Freiburg
Jensen S W 1978 *PhD Thesis* University of California, Riverside, California
Morrison M A, Lane N F and Collins L A 1977 *Phys Rev* A **15** 2186–201
Onda K and Truhlar D G 1979 *J. Phys. B: Atom. Molec. Phys.* **12** 283–90
Register D F, Trajmar S and Srivastava S 1980 *Phys Rev* A to be published
Shyn T W, Sharp W E and Carignan G R 1978 *Phys Rev* A **17** 1855–61
Srivastava S, Chutjian A and Trajmar S 1975 *J. Chem. Phys.* **63** 2659–65